



## Spherulite formation in obsidian lavas in the Aeolian Islands, Italy

Liam A. Bullock<sup>a, b, \*</sup>, Ralf Gertisser<sup>a</sup>, Brian O'Driscoll<sup>a, c</sup>

<sup>a</sup> School of Geography, Geology and the Environment, Keele University, Keele, ST5 5BG, UK

<sup>b</sup> Department of Geology & Petroleum Geology, Meston Building, University of Aberdeen, King's College, Aberdeen, AB24 3UE, UK

<sup>c</sup> School of Earth and Environmental Science, University of Manchester, Williamson Building, Oxford Road, Manchester, M13 9PL, UK

### ARTICLE INFO

Submitted: December 2016

Accepted: January 2017

Available on line: February 2017

\* Corresponding author:

liam.bullock@abdn.ac.uk

DOI: 10.2451/2017PM680

How to cite this article: Bullock L.A. et al. (2017)

Period. Mineral. 86, 37-54

### ABSTRACT

Spherulites in obsidian lavas of Lipari and Vulcano (Italy) are characterised by spatial, textural and geochemical variations, formed by different processes. Spherulites vary in size from <1 mm to 8 mm, are spherical to elongate in shape, and show variable radial interiors. Spherulites occur individually or in deformation bands, and some are surrounded by clear haloes and brown rims. Spherulites typically contain cristobalite ( $\alpha$ ,  $\beta$ ) and orthoclase, and rhyolitic glass, and grew over an average period of 5 days, with modification at lower temperatures. Heterogeneity relates to formation processes of spherulite 'types' at different stages of cooling and emplacement. Distinct populations concentrate within deformation structures, with variations in shape and internal structure. Crystal Size Distribution (CSD) plots show differing size populations and growth periods. Spherulites which formed at high temperatures show elongation, where deformation triggered further spherulite nucleation and growth. Spherulites formed at mid-glass transition temperatures are spherical, and spherulites are modified at vapour-phase temperatures. Enhanced undercooling, deformation, and modification are therefore pivotal in the development spherulite heterogeneity in obsidian lavas.

Keywords: Spherulites; Obsidian; Aeolian Islands; Glass Transition; Lipari; Vulcano.

### INTRODUCTION

Rhyolitic lava flows and domes on the islands of Lipari and Vulcano (Aeolian Islands, Italy; Figure 1) provide key information on the formation and modification of spherulites in obsidian lavas. This is in part due to their widespread occurrence, excellent exposure, and notable textural and geochemical variations. Despite their common occurrence in obsidian lavas worldwide, questions remain regarding the conditions and processes of spherulite formation. For instance, Watkins et al. (2008) highlight the open questions: on what timescale do spherulites form? When do spherulites begin to form? Do spherulites grow below the glass transition temperature bracket? Clay et

al. (2013) further stress the need for a detailed evaluation of the link between spherulite formation and deformation of obsidian lava flows. The preservation of spherulite textures in Aeolian Islands obsidian lavas presents a unique opportunity to classify spherulite heterogeneity, and identify processes responsible for their formation and variation.

Spherulites are radial fibrous crystallites, usually comprised of silica polymorphs and feldspar (Lofgren, 1971a; Swanson, 1977; McArthur et al., 1998; Gardner et al., 2012; Breitzkreuz, 2013). Spherulites are considered to progressively nucleate as a down temperature continuum during syn- and post-emplacement cooling (Clay et al.,



Figure 1. The Aeolian Islands, South Tyrrhenian Sea (Italy), with the islands of Lipari and Vulcano in the centre of the archipelago, straddling the Tindari-Letojanni fault system (Ventura, 2013).

2013), originally nucleating in response to an enhanced rate of undercooling brought on by degassing (Kirkpatrick, 1975; Swanson, 1977; Castro et al., 2009; Clay et al., 2013). As well as undercooling, plastic deformation following extrusion has also been suggested as a trigger for the formation of spherulites (Clay et al., 2013), and is particularly emphasised in organic and inorganic compounds and polymers (Shtukenberg et al., 2012). It is also suggested that spherulites form as a hydration and devitrification texture at lower temperatures (Lofgren 1971b; Swanson et al., 1989). It has been suggested that spherulite growth can occur above, within, and below the glass transition ( $T_g$  - 750-600 °C), whereby the material changes from liquid-like to solid via a viscoelastic phase transition (Ryan and Sammis, 1981; Manley, 1992; Davis and McPhie, 1996; Watkins et al., 2008; Gardner et al., 2012; Clay et al., 2013), meaning that emplacement mechanisms of obsidian lavas may play a key role in spherulite formation.

We report here a data set covering twelve obsidian lava flows and domes across Lipari and Vulcano, comprising 5405 individual spherulites, with the focus on the characterisation of their spatial distribution, textural features, and geochemistry. Spherulites have been classified in terms of their physical characteristics, chemical composition, and formation origin. Petrographic observations, mineral and glass geochemistry, laser Raman spectroscopy, X-ray diffraction (XRD) and Crystal Size Distribution (CSD) methods have been used in order to constrain spherulites formation in obsidian lavas in the Aeolian Islands obsidian suite. These observations and variations provide an indication of different processes of spherulite formation in Aeolian Islands obsidian lavas.

## GEOLOGICAL BACKGROUND

Recent activity in the central sector of the active Aeolian volcanic province has centred on rhyolitic activity,

involving both effusive and explosive phases. On the islands of Lipari and Vulcano, rhyolitic eruptions (often accompanied by mafic enclaves, e.g. De Astis et al., 1997, 2013; Davì et al., 2009, 2010; Piochi et al., 2009; Forni et al., 2013, 2015) have occurred from ~43 ka (Tranne et al., 2002; Gioncada et al., 2003; Lucchi et al., 2010, 2013; Forni et al., 2013), with the youngest eruptions occurring in historical time (Lipari - AD 776-1230; Keller, 2002; Forni et al., 2013; Vulcano - AD 1888-1890, Mercalli and Silvestri, 1891; De Astis et al., 2013). The oldest rhyolitic lavas are in southern Lipari (Punta del Perciato, Falcone, Monte Giardina and Punta di Costa lava domes; Figure 2), with younger domes in central and northern Lipari (Castello and Capo Rosso lava domes). At  $8.7 \pm 1.5$  ka ago, activity shifted further north on Lipari, with the Pomiciazzo obsidian lava flow extruded from the Vallone del Gabelotto eruptive vent (Bigazzi and Bonadonna, 1973; Lucchi et al., 2010; Forni et al., 2013; Figure 2). The extrusion of the Forgia Vecchia and Rocche Rosse obsidian lava flows mark the end of this most recent period of activity on Lipari, with the Rocche Rosse obsidian flow dated by archaeomagnetic methods at  $1,220 \pm 30$  AD (Tanguy et al., 2003), later revised to  $1,230 \pm 40$  AD (Arrighi et al., 2006; Figure 2). Rhyolitic lava flows and domes have also formed on the neighbouring island of Vulcano (De Astis et al., 1997, 2013; Piochi et al., 2009). The Grotta dei Palizzi obsidian lava flow on the southern flank of the active Fossa cone (Vulcano) has been dated at  $2.1 \pm 0.3$  ka (Voltaggio et al., 1995; De Astis et al., 2013; Figure 2), and, on the northern Fossa flank, the Pietre Cotte obsidian lava flow marks the latest outpourings of the 1739 AD activity (Frazzetta et al., 1984; Figure 2).

## SAMPLING AND METHODS

Targeted samples span rhyolitic lava domes ranging in age from  $43.0 \pm 0.3$  ka (Punta del Perciato, Falcone, Monte Giardina, Punta di Costa, Castello, and Capo Rosso lava domes on Lipari; Crisci et al., 1991; Lucchi et al., 2010; Forni et al., 2013), and younger lava flows (Pomiciazzo, Grotta dei Palizzi, Forgia Vecchia, and Rocche Rosse lava flows on Lipari and Vulcano; De Astis et al., 2010; Forni et al., 2013), to the 1739 AD activity (Pietre Cotte lava flow on Vulcano; Frazzetta et al., 1984) (Figure 2). Samples from younger obsidian lavas generally host better-preserved spherulites, and were therefore more extensively sampled. Samples were cut for thin section, and scanned for spherulite CSD analyses. A thickness of one device pixel in width was used. Processing programs *ImageJ* (Schneider et al., 2012), *CSDSlice* (Morgan and Jerram, 2006), and *MATLAB*® 6.1 commercial software were used to analyse all particles in a given image, including total spherulite count, spherulite phase abundance, and best fit spherulite shape. *CSDSlice* calculates a best fit for the aspect ratios, giving X, Y and Z

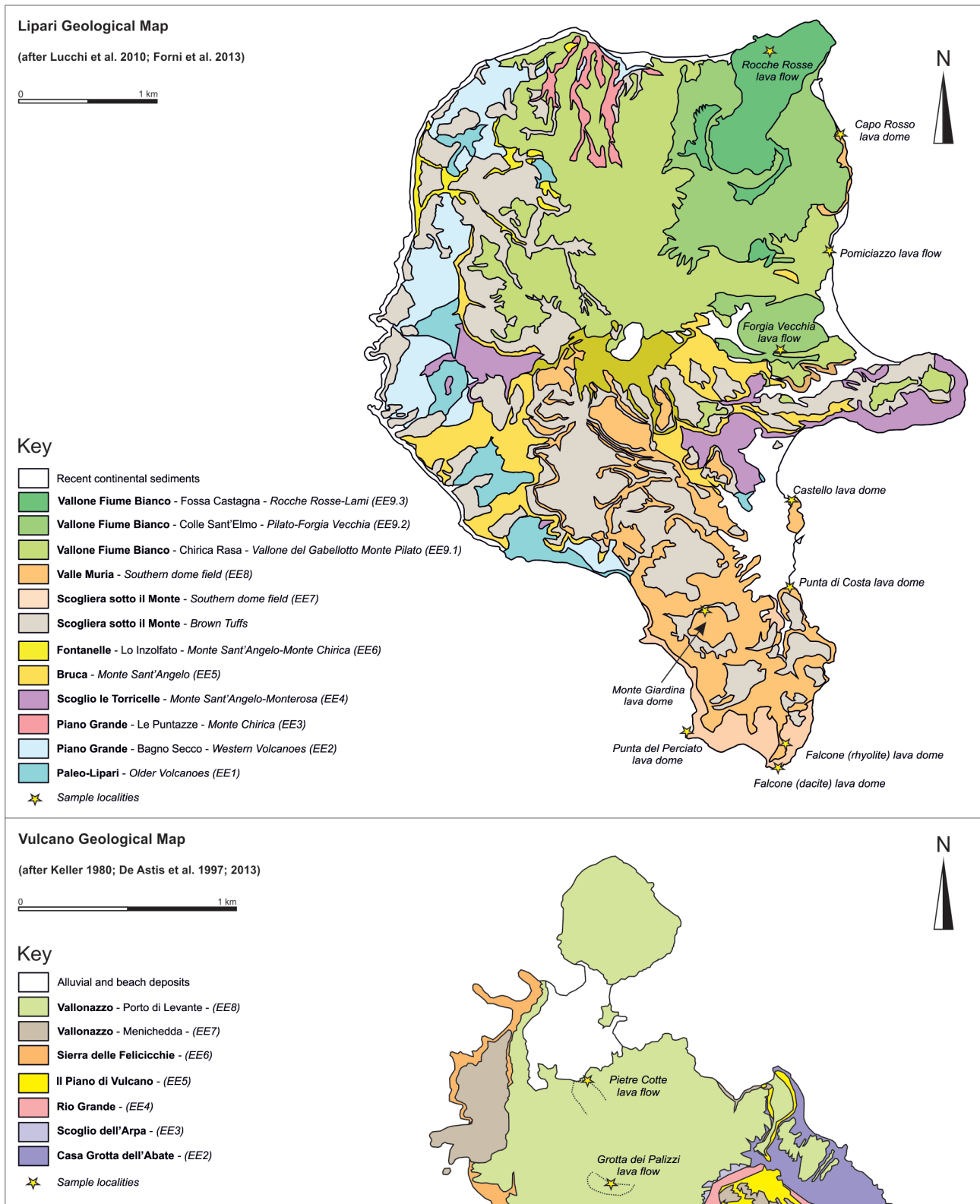


Figure 2. Geological maps and sample locations of obsidian lavas on Lipari and Vulcano (after Keller, 1970; Pichler, 1976; Lucchi et al., 2010; De Astis et al., 2013; Forni et al., 2013). Units classified by synthems, subsynthems and eruptive history as defined in the geological map of Forni et al. (2013), with synthems shown in bold text, subsynthems in normal text, and eruptive epochs in italics.

values (defining the plane in a 3D space). *CSDCorrections 1.37* (Higgins, 2000, 2002, 2006), was used in order to calculate 3D crystal size distributions from 2D data.

Glass and mineral major element analysis was undertaken at The Open University (UK) using a CAMECA SX 100 electron microprobe (EMP). The peak count per element for analyses was 15-30 s using a 10-20  $\mu\text{m}$  defocused beam diameter for glass (a 1  $\mu\text{m}$  wide beam was used for minerals at a count time of 40 s per element), with an acceleration voltage of 15 kV and a beam current of 20 nA for glass and minerals. Volcanic glass standards (VG-568 and KN-18) were routinely analysed as secondary standards. For XRD determination of individual compositional phases, spherulites were crushed and sieved, hand-picked using a binocular microscope, and powdered. The coarsely-powdered samples were placed on a flat disk sample holder, gently compressed, and scanned on a Bruker D8 Advance X-ray diffractometer, equipped with a VÅNTEC-500 detector at Keele University (UK), using  $\text{CuK}\alpha$  radiation, a scan range from 5 to 90° (2 Theta), a 0.03° (2 Theta) step size and a data collection time of 10 s per step. Samples were prepared for Raman analysis by being cut to wafer-thin sections, ~20  $\mu\text{m}$  in thickness, and polished on both sides. Specific positions in the glassy groundmass, spherulites and brown rims were targeted using a high magnification petrological microscope. Spots of glassy groundmass free of microlites and alteration were targeted. Laser Raman spectroscopy analyses were performed with a Leica microscope coupled to a Renishaw Raman RM1000 system at the University of Southampton (UK), using a Renishaw NIR 780TF semiconductor diode laser (wavelength 780 nm) of power 25 mW. The spectrometer was set up in line with Renishaw recommendations for confocal operation of the spectrometer, calibrated using silicon with a known peak of 520  $\text{cm}^{-1}$ . Spectra were obtained using an extended scan between 3700  $\text{cm}^{-1}$  and 100  $\text{cm}^{-1}$ , built up of 9 accumulative scans of 10 s, with a spot size of 1-2  $\mu\text{m}$ , and processed using *SigmaPlot 10*.

## RESULTS

Important characteristics in sampled obsidian lavas include variable deformational structures, degree of devitrification, spherulite morphology, and glass and spherulite geochemistry. These characteristics may impact (or trigger) spherulite nucleation, growth, and modification. CSD methods were utilised in order to assess physical and spatial features, while EMP, XRD, and Raman spectroscopy methods provide a means of geochemical characterisation of spherulites and host glass.

### Textural observations

A number of well exposed lava flows and domes show brittle and ductile deformational fabrics, with multi-scale

folding, stretching lineations, and sheared spherulites evident (Figure 3). Such deformational structures often coincide with areas of high spherulite density, and elongate spherulites. Deformational fabrics are widespread across the Rocche Rosse lava flow, whereas deformed fabrics are more restricted to flow frontal regions and flow margins on the Pietre Cotte lava flow (Bullock, 2015). Structures in older lava domes are more difficult to distinguish due to weathering, glass alteration, and later pyroclastic coverage.

Optical observations of sampled obsidian lavas suggest distinct textural features within the obsidian samples, including widespread spherulites, a glassy groundmass containing microlites, a brown rim and clear halo surrounding most spherulites, and a crystalline mesh-texture found within some spherulites (Figure 4). Sampled obsidian across the data set is typically glassy black to microcrystalline grey in colour, and variably spherulitic (spherulites predominantly less than 1 mm in diameter, and often defining the planar foliation). Spherulites occur individually, interjoined, and in folds and fractures (Figure 4). Elongate spherulites can be observed in the Pietre Cotte, Rocche Rosse and Forgia Vecchia lava flows. These elongate spherulites tend to occur within or in close proximity of bands or folded outcrop. Generally, across all flows and domes, large (1-3 mm), spherical spherulites occur individually in zones of low shear or in zones of no banding. Spherulites in the Pomiciazzo and older sampled lavas tend to be much larger than those in younger flows, at 2-3 mm in diameter. The Punta del Perciato lava dome is highly devitrified, and individual spherulites are rarely evident to the naked eye.

### Spherulite CSDs and growth periods

Clay et al. (2013) show that CSD quantitative textural analysis can be successfully applied to spherulitic samples, as the rate of isothermal spherulitic crystallisation was proven to be log linear in a given growth stage, despite being a non-equilibrium crystallisation process. The use of CSD methods is therefore an effective tool for the interpretation of spherulitic textures. Twelve CSD plots of spherulites from all lava flows and domes have been produced, with spherulites ranging in size from 0.1 mm (in younger flows), up to 8 mm (in older domes) (Figure 5). Overall, the sample set shows a kinked regression profile, with steeper, left-hand truncation at lower spherulite sizes, and a shallowing, more uniform regression to larger spherulite populations. The majority of plots show a higher degree of heterogeneity at smaller spherulite sizes, while some plots show little or no deviation from a log-linear profile. Older sampled domes exhibit larger spherulite maximum sizes and wider size ranges. Spherulites below 1 mm in size show a greater degree of complexity, evident by highly non-linear slope regressions. With the exception of samples from Castello,

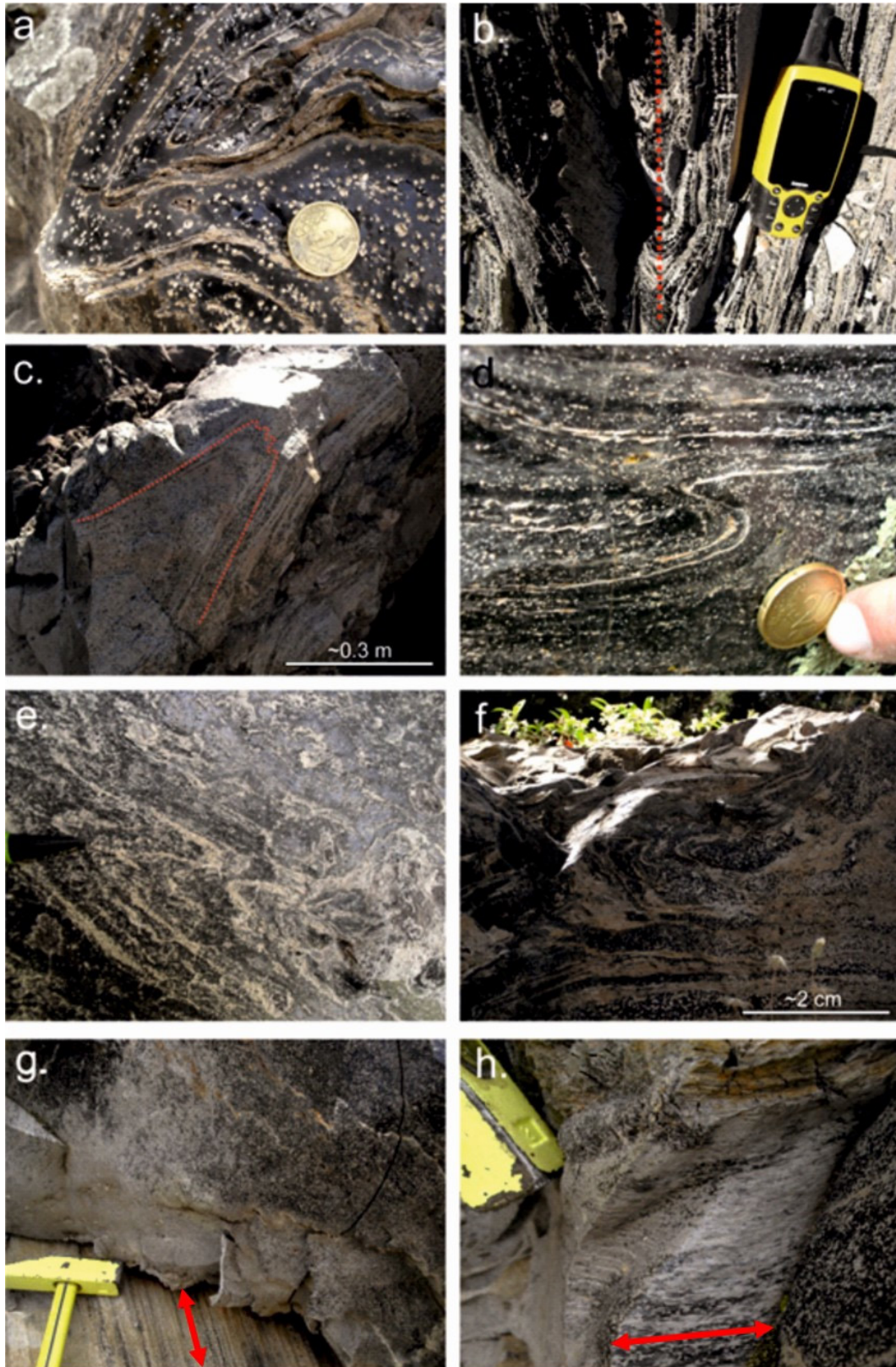


Figure 3. Evidence for spherulitic obsidian coinciding with areas of flow deformation, including (a)-(f) compressive folding (red line in b. highlighting the fold axial plane, and in c. representing fold outline) and (g)-(h) structures resulting from constrictional forces (arrows indicate stretching lineations).

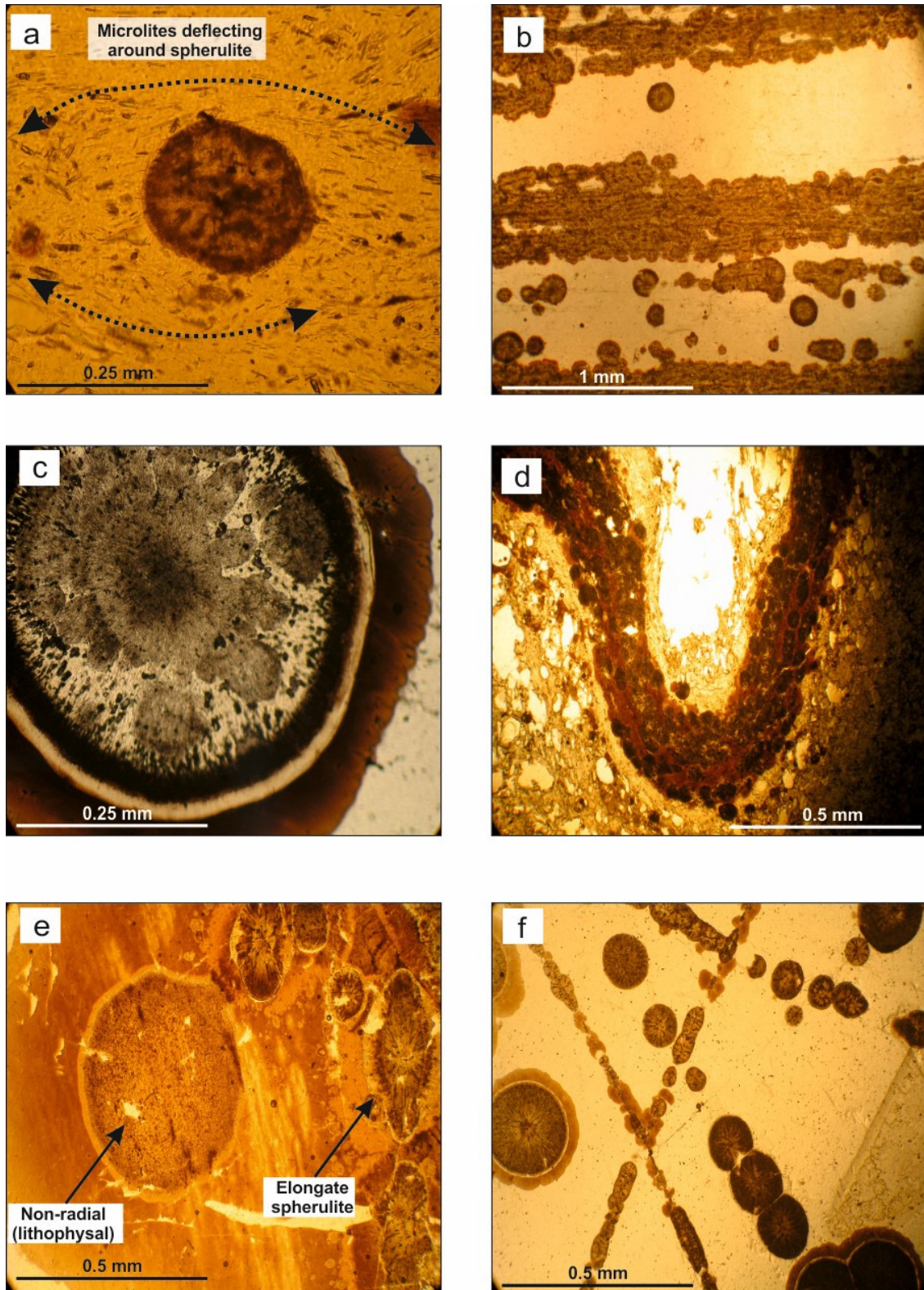


Figure 4. (a) Small spherulite (Pietre Cotte), with aligned microlites deflected. (b) Spherulites defining flow foliation, heavily concentrated within bands, with few spherulites in zones of low shear (Rocche Rosse). (c) Spherulite with radial centre, mesh-texture near edge, outer clear halo and surrounding brown rim (Falcone rhyolite). (d) Microscopic folding, with folded spherulitic-rich band (Rocche Rosse). (e) Microcrystalline spherulite (non-radial) and ellipsoidal, radial spherulites (Pomiciazzo). (f) Spherulites concentrated within conjugate fracture (Rocche Rosse).

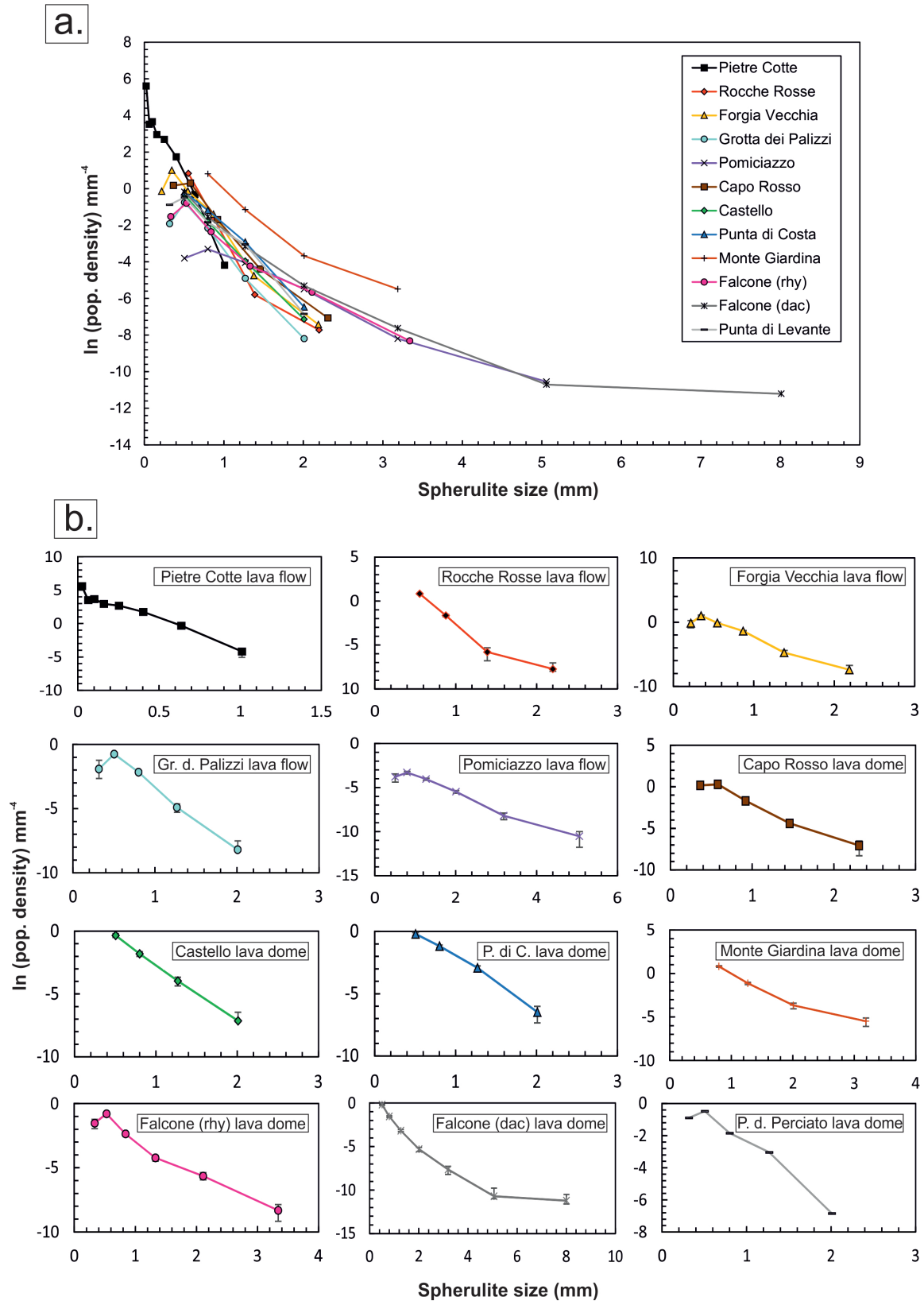


Table 1. Spherulite crystal size distribution (CSD) parameters for sampled lava flows and domes. Calculated growth periods for spherulite growth are also shown in the table (small and large size fractions removed and calculated through the main body of the CSD). Growth period based on a growth rate of  $6.33 \times 10^{-7} \text{ m s}^{-1}$  (calculated by Castro et al., 2008).

Flow/dome	No. of spherulites	Y intercept	Slope value	R <sup>2</sup> value	Short axis	Int. axis	Long axis	Sphericity (%)	Growth period (days)
Pietre Cotte	999	4.7997	-8.5831	0.9826	1	1.4	2.8	56.3	2.1
Rocche Rosse	451	5.2683	-7.9464	0.9998	1	1.05	1.15	92.6	2.3
Grotta dei Palizzi	154	1.7185	-4.9954	0.9966	1	1.05	1.05	98.4	3.6
Forgia Vecchia	395	2.4416	-4.6717	0.9838	1	1.15	1.25	90.3	4
Pomiciazzo	255	-1.9983	-1.7524	0.9859	1	1.05	1.05	98.4	10.4
Capo Rosso	446	2.3387	-4.2148	0.9793	1	1	1.15	91.1	4.3
Castello	130	1.8541	-4.5033	0.9992	1	1	1	100	4.1
Punta di Costa	431	2.1136	-4.1954	0.9933	1	1.05	1.05	98.4	4.4
Monte Giardina	326	2.3264	-2.5891	0.9489	1	1	1	100	7.1
Falcone (rhyolite)	576	-1.4589	-2.0418	0.9943	1	1.05	1.1	95.4	8.9
Falcone (dacite)	1086	1.2866	-3.3478	0.9912	1	1.05	1.05	98.4	5.5
Punta del Perciato	156	1.0329	-3.2901	0.9717	1	1	1	100	5.6

Punta di Costa and Monte Giardina, CSD slopes for sampled flows and domes often deviate from a straight line regression. Slopes show a distinct smaller population at <1 mm (Pietre Cotte, Forgia Vecchia, Grotta dei Palizzi, Pomiciazzo, Capo Rosso, Falcone rhyolite, and Punta del Perciato), a slope at intermediate sizes of 1-3 mm (Rocche Rosse, Falcone rhyolite, Falcone dacite, Punta del Perciato), and a shallower slope to larger spherulite sizes (Pomiciazzo, Falcone rhyolite, Falcone dacite).

Spherulite growth period was calculated using the CSD slope value (determined by *Microsoft Excel*), and assuming a constant spherulite growth rate of  $6.33 \times 10^{-7} \text{ m s}^{-1}$  (calculated by Castro et al., 2008, in obsidian using water concentration profiles). The equation for calculating growth period is:

$$\text{Growth period} = -1 \div (\text{slope value} \times \text{growth rate})$$

(Marsh, 1988, 1998)

The average spherulite growth period across all individual slopes is ~7 days. However, larger spherulites may have formed due to modification/re-crystallisation processes occurring post-emplacement, and therefore may not be a true reflection of primary spherulite growth. Calculating growth periods from smaller and larger size

fractions is also difficult as these are typically only defined by two bin sizes. Therefore, small and large size fractions were excluded from calculations, and the slope value was extracted from the main linear body of the CSD profile, defined by three or more bin sizes. If slopes representing smaller and larger spherulites are excluded, the average growth period is ~5 days. Growth periods range across samples from 2 to 11 days (Table 1). A growth period has been calculated for smaller spherulites, though this is only tentatively suggested as the size fraction is defined by only two bins. Based on this estimation, smaller spherulites (distinct population < 1 mm) formed on average in less than a day. Intermediate spherulites (~1-3 mm) formed over an average of ~5 days (growth periods ranging 2-7 days based on the main body of the CSD profile). Linear slopes from Castello, Punta di Costa and Monte Giardina samples (spherulites typically ~1-3 mm in size) indicate that these spherulites also typically formed over ~5 days, with a range of 4-7 days.

#### Glass and spherulite geochemistry

All glass and mineral compositional data is provided in the Supplementary Appendix. The glass compositions range from rare dacitic/trachytic to typically rhyolitic. The minimum SiO<sub>2</sub> content is ~68 wt% (the Falcone lava dome



and Punta del Perciato lava dome), and the maximum  $\text{SiO}_2$  content is  $\sim 79$  wt% (also from the Falcone lava dome) (Figure 6). The average  $\text{SiO}_2$  content for the obsidian glasses is  $\sim 75$  wt%.  $\text{Al}_2\text{O}_3$  content varies from  $\sim 11$  wt% to  $\sim 19$  wt% (averaging  $\sim 13$  wt%). Typical  $\text{Na}_2\text{O}$  content is  $\sim 3$ - $5$  wt%, with slightly higher  $\text{Na}_2\text{O}$  content in the Grotta dei Palizzi lava flow ( $\sim 5$ - $6$  wt%). Brown rims surrounding spherulites show variable enrichment and depletion of  $\text{SiO}_2$ ,  $\text{Na}_2\text{O}$  and  $\text{K}_2\text{O}$ . Generally, spherulites show a high Si content, and a relatively high Al and K content, in specific phases (with a skeletal crystal arrangement). Electron microprobe spot analyses of spherulites reveal a mixture of phases, including glass (with silica values between  $\sim 70$  wt% and  $\sim 78$  wt%), and cristobalite (silica content of  $\sim 99$  wt%), and orthoclase (silica content 60-67 wt%). Spherulites in all sampled obsidian flows and domes contain orthoclase and a silica phase. Plagioclase identified by EMP is primarily albitic.

Examination of Raman spectra for the glassy obsidian groundmass, spherulites (including the microcrystalline mesh-texture) and brown rims show minimal variation in notable peaks (Figure 7). Spectral results for the haloes show some slight variations. Sharp peaks represent the presence of rare crystalline material, and the broad humped regression is characteristic of amorphous material. Peaks at  $\sim 460$   $\text{cm}^{-1}$  and  $\sim 510$   $\text{cm}^{-1}$  confirm the presence of silica and orthoclase in spherulites and the glassy groundmass (microlites). There are also notable peaks at  $\sim 230$   $\text{cm}^{-1}$  and  $300$   $\text{cm}^{-1}$ , with a relatively flat area between  $800$   $\text{cm}^{-1}$  and  $1200$   $\text{cm}^{-1}$ . Spherulites, mesh-textured interiors and surrounding brown zones show a similar trend to the glassy matrix, confirming the presence of rhyolitic glass in

spherulites. Despite the differing optical properties (non-isotropic under crossed polarised light), the brown rims show the characteristic profiles akin to a glass response. The main difference between glass and brown rim results is that although the brown rim shows an amorphous hump appearance, peaks tend to be sharper (more akin to crystalline material). The two major XRD peaks at  $21.6^\circ$  and  $27.3^\circ$  ( $2\theta$ ) correspond to  $\alpha$ -cristobalite and orthoclase feldspar respectively, with minor peaks representing diopside (Figure 8). There are also peaks suggesting trace amounts of  $\beta$ -cristobalite, diopside and titanomagnetite, with peaks varying in occurrence and intensity across sampled lavas.

## DISCUSSION

### Textural variations in spherulites

Results suggest that the sampled obsidian suite across Lipari and Vulcano host spherulite populations of heterogeneous textural characteristics. This is evident in both petrographic observations and kinked CSD profiles (Figure 6). The upward kinking profile of the CSD plots indicates increasing heterogeneous spherulite nucleation, e.g. faster or denser spherulite nucleation at a later stage. Distinct CSD slopes reflect individual spherulite populations, nucleating and growing at different times and at different rates. This results in texturally heterogeneous spherulite populations within an obsidian lava. In some instances, there is evidence for a downturn at the smaller spherulite sizes (Figure 6). Petrographic observations suggest that spherulites do not occur below the resolution limit, and smaller spherulites are optically distinct compared to larger spherulites. For

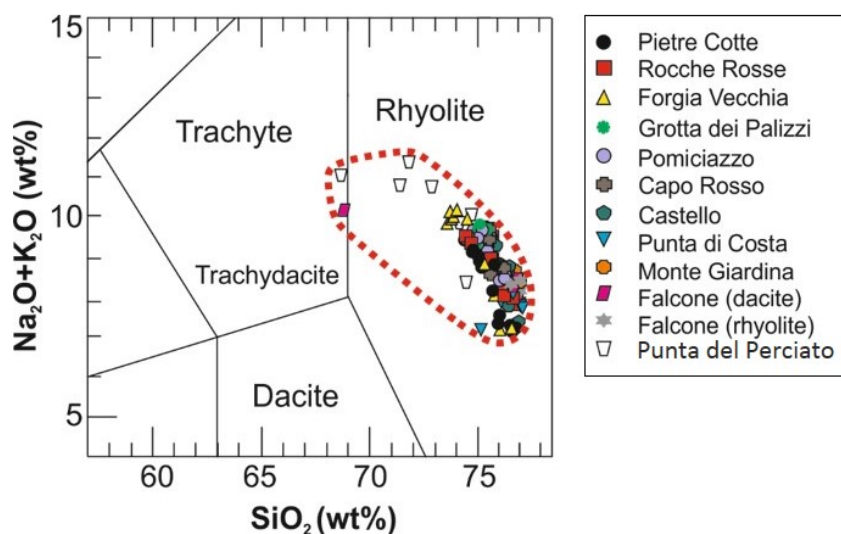


Figure 6. Total Alkali-Silica (TAS) diagram (adapted from Le Bas et al., 1986) of glass compositions across sampled lavas. The majority of points are clustered together at 73-76 wt%  $\text{SiO}_2$  and 7-9 wt%  $\text{Na}_2\text{O} + \text{K}_2\text{O}$  (shown by red field).

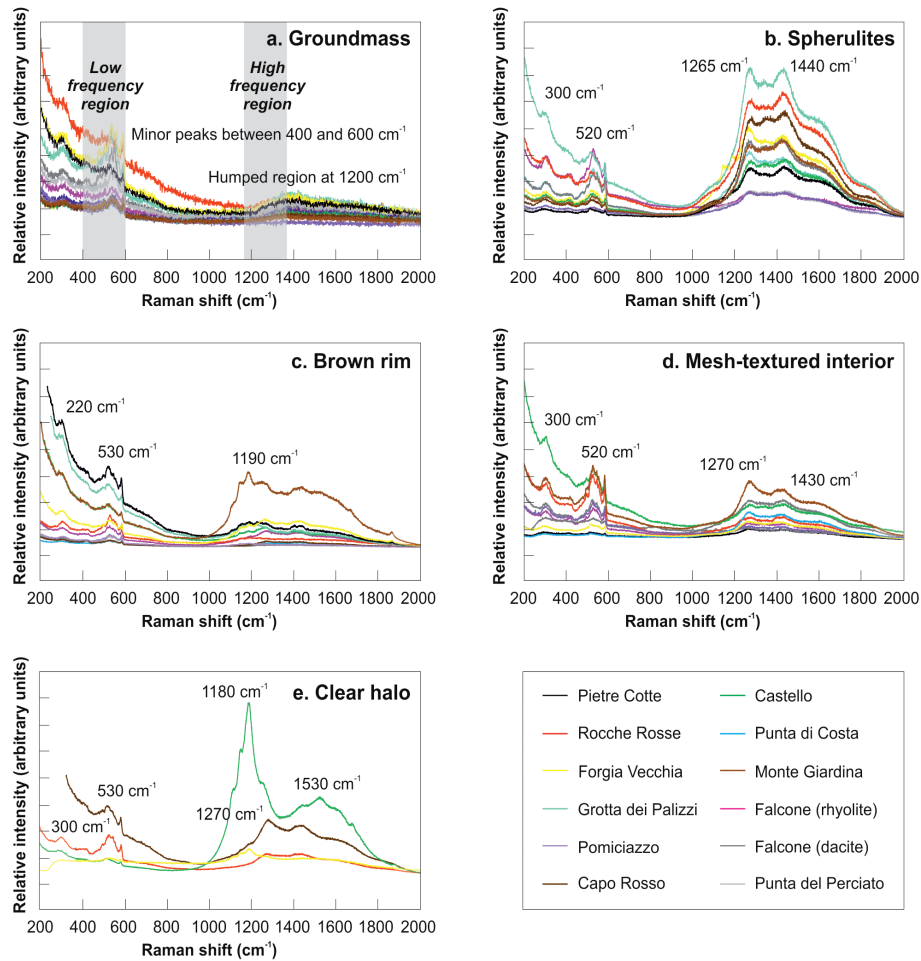


Figure 7. Raman spectrum and peaks for (a) obsidian glass groundmass, (b) spherulite interiors, (c) brown rims surrounding spherulites, (d) mesh-like textures found in some spherulites, and (e) clear haloes immediately surrounding some spherulites.

spherulites, the upward inflection suggests a clustering or coalescence of large spherulites, the result of localised high nucleation rates and/or the product of prolonged devitrification. Later-stage vapour-phase crystallisation overprinted or re-crystallised earlier formed spherulites, evident by lithophysal textures with an original spherulite in the centre, and resulting in a greater population density of larger spherulites. Samples exhibiting a simple log-linear regression slope indicates a single nucleation event, likely to be the result of constant undercooling. Generally, younger flows have shorter growth periods, and older domes have longer growth periods. This may be a reflection of the size of spherulites being a function of a constant growth rate. However, spherulites are likely to grow at a different rate in a melt compared to those growing in a semi-solid or solid obsidian state. Spherulites may also have grown at different rates from different spherulite-forming processes, i.e. spherulites growing at high temperatures as a response to enhanced undercooling, and spherulites nucleating and growing as a

result of deformation. Calculated growth periods for older samples may also take into account the effects of late stage infilling phases (Holzhey, 2001). Notable exceptions to spherulite size being primarily a function of time are large spherulites in samples from the Pomiciazzo lava flow and the Falcone dacite lava dome. As well as time, spherulite growth is primarily a function of temperature and flow rheology. At temperatures approaching melting point, molecular stems settle for longer on the growing crystal face, thus allowing spherulites to grow faster (Lauritzen and Hoffman, 1973; Hoffman et al., 1975; Hoffman and Miller, 1997). Growth may also relate to viscosity, with high  $T_g$  viscosities inhibiting diffusion, and thus reducing spherulite growth rate. This suggests that larger spherulites observed in Pomiciazzo and Falcone dacite samples may be a result of differential systems exhibiting prolonged period of higher temperatures and lower viscosities.

The regular and highly recognisable occurrence of densely spherulitic glass coinciding with flow deformation, and the uniform occurrence of elongate

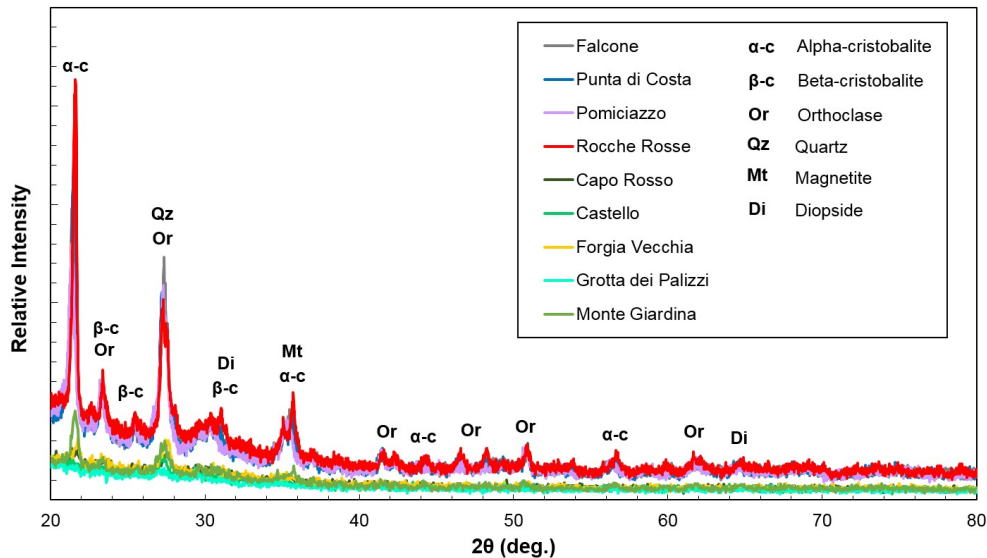


Figure 8. X-ray diffraction (XRD) results and peaks for spherulites from sampled lavas. Notable peaks include several  $\alpha$ -cristobalite and orthoclase peaks (main constituents), with minor magnetite,  $\beta$ -cristobalite, and diopside peaks.

and/or sheared spherulites, supports a link between flow deformation and spherulite nucleation. Flow-induced crystallisation, also referred to as flow-enhanced nucleation or shear-enhanced nucleation (Graham and Olmsted, 2009), is a well understood phenomenon in polymer sciences as a trigger for spherulite nucleation, but is thus far a neglected concept in a geological context. Elongation in an extensional flow regime has been cited as a strong stimulus for polymer crystallisation, causing molecules to orient and stretch in the direction of extension, facilitating the process of flow-induced crystallisation (Janeschitz-Kriegl et al., 2003; Kornfield et al., 2002; Stadlbauer et al., 2004). Shear flow can induce crystallisation, requiring very large generation of strain (Derakhshandeh and Hatzikiriakos, 2012). Extension and shear flow-related crystallisation may therefore be applicable in highly deformed obsidian lavas. Nucleation depends on the change of the free energy difference between the crystal and the melt phases; the degree of order in the melt phase increases under shear conditions, and the free energy difference increases. The entropic penalty for crystallisation is lowered and, therefore, the nucleation rate increases (Keller and Kolnaar, 1997; Coccorullo et al., 2008). This leads to a high number density of spherulites as a result of deformation, which is evident in field observations in obsidian lavas. This may suggest that, in obsidian lavas, spherulite nucleation may increase with flow deformation (during flow), and remain constant in areas of low (or no) strain (e.g. in areas unaffected by strain during flow, or following flow cessation). This results in high spherulite populations in areas of high strain (and spherulites may be sheared or elongate as a result, also observed in the Rocche Rosse

lava flow by Clay et al., 2013), and lower populations of (undeformed) spherulites in zones of low strain, allowed to grow and form more typical spherical shapes.

Elongate spherulites (elliptical as opposed to bowtie shaped) spatially found within close proximity to deformational structures in sampled flows and domes may have formed while lava was behaving in a ductile manner (within  $T_g$ ). This is similar to how vesicles and enclaves preserve lava flow strain, based on their shape and size alteration from spherical to elongate (Polacci and Papale, 1997; Rust et al., 2003; Ventura, 2004; Iezzi and Ventura, 2005). The onset of this spherulite nucleation and growth may therefore have been triggered (or enhanced) by flow-induced crystallisation (i.e. as a result of deformation) at high  $T_g$  temperatures. This is supported by polymer experiments whereby flow-induced crystallisation occurs near melting point (above  $T_g$  or high  $T_g$  transition) (Binsbergen, 1966). The stress created by both spherulite nucleation and that acting due to lava flow emplacement modifies the spherulite shape from spherical to elongate. In zones of high strain, such as at flow margins or where individual flow lobes overlap, spherulites are completely sheared into fully spherulitic bands, or microlite-rich flow bands (which may have resulted from flow-induced crystallisation) became spherulite-rich due to microlites acting as spherulite nuclei. There is also clear evidence for spherulites nucleating and growing within brittle fractures, such as conjugate fractures and tension gashes. This suggests that spherulites have preferentially nucleated in these fractures while the flow is behaving in a brittle manner, i.e. at low or below  $T_g$  temperatures in localised regions of flow or due to high strain rate, as a response to deformation.

### Geochemical variations in spherulites

The presence of trace amounts of high temperature  $\beta$ -cristobalite suggests that spherulites were forming at least higher than the  $\beta$ - $\alpha$  temperature transition (~270-200°C; Wright and Leadbetter, 1975; Downs and Palmer, 1994; Swainson and Dove, 1994; Damby et al., 2014), as a quench phenomenon (Ewart, 1971). Spherulites were likely to begin forming early, with high temperature  $\beta$ -cristobalite converting to low temperature  $\alpha$ -cristobalite (in some instances, incomplete conversion resulting in both  $\alpha$ - and  $\beta$ - cristobalite). These phases are identified in the XRD peaks. Variations in the intensity and shift of peaks in the clear surrounding haloes results may suggest some degree of compositional variation (evident in EMP results), and may relate to different processes forming the haloes, e.g. secondary crystallisation infilling (Breitkreuz, 2013), or Fe-redox shift (Castro et al., 2009).

Results suggest some depletion and enrichment of major elements within spherulites relative to the glassy matrix, and a surrounding rim. Following initial spherulite growth, cavities at the interface of the spherulite and surrounding material may open out, which act as a nucleation surface for a second phase of crystallisation (Breitkreuz, 2013). Where the surrounding halo does not show a crystalline interior, the surrounding colourless halo may be enriched in OH groups and depleted in ferric iron, produced by a redox front (driven by magnetite crystallisation) that originated from the spherulite margin (Castro et al., 2009). Low-temperature components which are rejected at the crystal-melt interface, assisted by a low diffusion rate, form an impurity layer (Keith and Padden; 1963; Lofgren, 1971b). This impurity layer may be identifiable in Aeolian Islands obsidian samples as the surrounding colourless halo or brown rim evident across all lava bodies. The presence of glass within spherulites is reported here, and also noted elsewhere (e.g. Richnow, 1999; Ryabov and Grib, 2005; Castro et al., 2008, 2009; Seaman et al., 2009; Gardner et al., 2012). Seaman et al. (2009) conclude that the preservation of glass within spherulites highlights the critical influence of water concentration on the likelihood of quenching versus crystallisation during undercooling of a melt. Richnow (1999) also suggests that the presence of glass within spherulites is an indicator of incomplete crystallisation and spherulite formation above  $T_g$  temperatures.

### Processes of spherulite formation in Aeolian Islands obsidian lavas

As rhyolitic lava cooled, it passed from liquid-like behaviour to solid (glass)-like behaviour (Gottsmann and Dingwell, 2001b). Nucleation and spherulite formation originally occurred as a response to undercooling, and continued as a down-temperature growth continuum (Clay et al., 2013). In the majority of sampled lavas, microlites grew first and were later overgrown by

spherulites. Therefore spherulites mainly formed at lower temperatures than microlite crystallisation. However, smaller spherulites sometimes show microlites deflected around them, indicating that spherulites grew at higher microlite crystallisation temperatures. Spherulites which exhibit a radial centre and non-radial outer zone preserve evidence for both primary spherulite crystallisation and lithophysae forming processes. Spherulites are often surrounded by a brown rim, but there are smaller spherulites which do not show this rim. These spherulite rims may have formed within or below  $T_g$  as a solid state reaction (Castro et al., 2009).

Textural observations, geochemistry and CSD plots suggest that multiple spherulite populations exist across obsidian flows and domes on Lipari and Vulcano. Each population can be classified according to their textural heterogeneity (Figure 9). From the digitised spherulites, a representative shape for each spherulite type was created using the CSDSlice program of Morgan and Jerram (2006). X, Y and Z values were plotted in MATLAB® 6.1 in order to provide a representative 3D sphere for each spherulite type (Figure 9). Here, the X, Y and Z data were scaled with the radius, with the centroid of sphere representing 0 on each of the three axes. The equal square axes allow for direct comparison of representative spherulite type shapes, and show true elongation. Representative shapes show that early, high temperature spherulites are more deformed than later, lower temperature spherulites, peaking at high  $T_g$  temperatures, with deformation waning towards lower  $T_g$  temperatures and below. Initial spherulite nucleation and growth may have been triggered by enhanced undercooling above  $T_g$ . This results in spherulites with radial interiors. These can be classified as type 1 spherulites. Microlites were deflected by these high temperature spherulites. Type 1 spherulites are typically the smallest spherulite types (responsible for left hand truncation in spherulite CSDs). The formation of spherulites during emplacement at high  $T_g$  transition results in elongate (or sheared) spherulites during ductile flow deformation, which are classified here as type 2 spherulites. The occurrence of isolated, spherical spherulites (larger than type 1 spherulites) with a brown rim suggests that some spherulites formed in areas of low strain. These are classified as type 3 spherulites. Other spherulites grew at temperatures within and below  $T_g$ , and concentrated within fractures or bands (deformational trigger), classified as type 4 spherulites. Hollow, partially-hollow, or spherulites containing tensional voids and cavities later became infilled or re-crystallised, resulting in internal spherulite colour zonation and pockets of crystal phases. These are classified as type 5 spherulites (modification of other spherulite types), and may only partially contain a radial texture or no radial texture at all. During ascent, eruption and emplacement, lava is likely

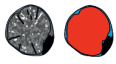
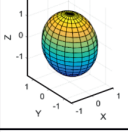
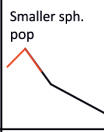

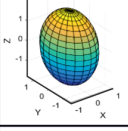
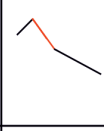

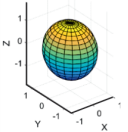
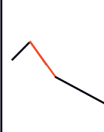

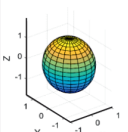
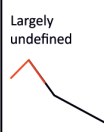

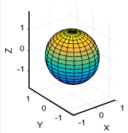
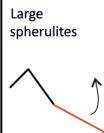
Type	Image	Representative shape	Typical size	Features	Composition	Growth period	% of total sph.	% of total sph. area	Typical CSD slope	Formation
1	 Small, radial, slightly elongate		< 1 mm	Radial interior, sub-spherical, occasional mesh-textured rim, microlites deflected	a-β cristobalite transition (some β crist. fixed in matrix), orthoclase, glass, diopside, titanomagnetite	Less than one day	19.3%	3%		Enhanced undercooling at high T temperatures above $T_g$ (temperatures similar to microlite crystallisation)
2	 Elongate		1-2 mm	Elongate shape, vague radial interior, associated with deformational fabrics, brown rim, mesh-texture	a cristobalite, orthoclase, glass. Zones and pockets of pure crystalline silica	2-7 days	10.2%	13.3%		Constant degree of undercooling and deformational trigger. Nucleation during high $T_g$ temperatures
3	 Radial, large and spherical		1-3 mm	Radial interior, sub-spherical, associated with zones of low shear, clear halo, mesh-textured rim, thick brown rim, microlites unaffected	a cristobalite, orthoclase, glass. Zones and pockets of pure crystalline silica	2-7 days	51.9%	39.4%		Constant enhanced undercooling and deformational trigger (low intensity), mid to sub $T_g$ temperatures
4	 Conjugate fracture		<1 mm	Concentrate within joints and fractures, often interjoined, no halo or brown rim, radial and no zonation	a cristobalite, orthoclase, glass	-	5.3%	2.8%		Deformation and preferential nucleation within constrained faults and fractures, below $T_g$ , nucleation and restricted growth (spatially-controlled)
5	 Lack of internal structure		>1 mm	Partially radial or microcrystalline interior, non-continuous or poorly defined spherulite edge, mesh-like texture	a cristobalite, quartz, orthoclase, glass	-	13.4%	41.7%		Modification of previous types at vapour stage temperatures and below $T_g$ , secondary alteration of spherulites and cavities. Otherwise classified as lithophysae

Figure 9. Spherulite type classification scheme based on textural characteristics, composition, and CSD plots. In the digitised images, red areas represent a primary spherulite phase, blue is a secondary infilling phase, and yellow is a reaction rim.

to cross  $T_g$  many times, resulting in breaking, flowing, and healing in repetitive cycles (Tuffen et al., 2003; Tuffen and Dingwell, 2005; Vasseur et al., 2013). As a result, spherulites types formed concomitantly in different parts of the obsidian lava body, relating to temperature variations and different processes at work (e.g. at higher temperatures in the core of the obsidian lava, or as a result of flow-induced crystallisation).

Though spherulite formation is a function of processes such as undercooling and deformation, it is unlikely to be fully time constrained. Repeated fracturing and healing of rhyolite (Gonnermann and Manga, 2003; Tuffen et al., 2003; Tuffen and Dingwell, 2005; Vasseur et al., 2013), and second boiling (separation of a gas from a liquid phase) also occur (Manley and Fink, 1987; Westrich et al., 1988; Sisson and Bacon, 1999; Tuffen et al., 2012), which may re-initiate crystallisation. Therefore, differing spherulite types may nucleate and form simultaneously (Figure 10). Rheological properties such as elasticity and temperature are intrinsically linked. Such rheological parameters will differ across lava flows and domes during and after emplacement. It can therefore be assumed that deformation is intrinsically linked with temperature

and different spherulite types form at the same time. In an obsidian flow, for instance, it will be cooler at flow margins and hotter in the centre of the flow. Therefore, spherulites forming via high temperature undercooling in one part of obsidian lava (such as the core of the flow) do so concomitantly with spherulites forming during  $T_g$  in other parts of the lava (by flow-induced crystallisation at margins). Type 5 spherulites, characterised by modification and filling of cavities, may occur during and after vapour-activity and fracturing. Such recrystallisation textures developed due to primary cooling, and continued throughout the cooling history of the lavas. Repeated fracturing and healing also means that type 4 spherulites cannot be fully time-constrained, but are restricted to areas of flow that are undergoing a brittle flow regime.

### Spherulite growth and modification

A total of 5405 spherulites were digitised according to their designated type, from samples spanning all sampled lavas (Figures 9 and 11). Type 3 showed the highest population of spherulites (51.8%). Types 1, 2 and 5 show a similar percentage of the total population (19.3%, 10.1% and 13.4% respectively), and type 4 was the lowest

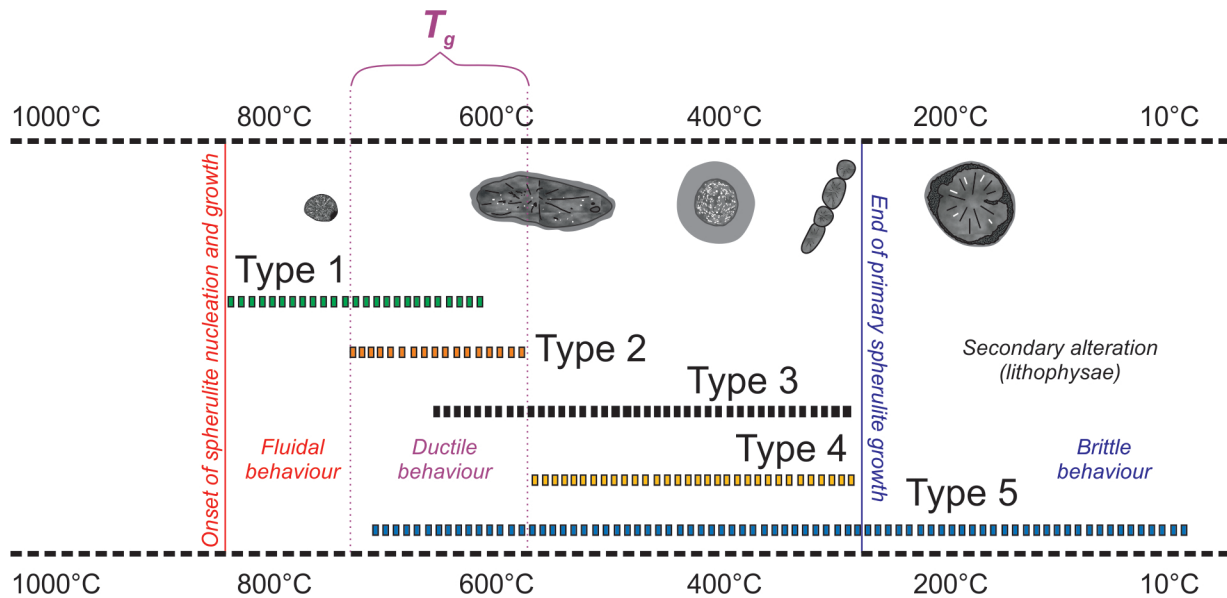


Figure 10. Temperature model for the formation of classified types of spherulites (texture process timeline modified from Breitreuz, 2001). Model demonstrates that spherulite type classification is rheologically controlled, and spherulite types may form simultaneously in different areas of lava. Indicated  $T_g$  range is based on previous estimations (Ryan and Sammis, 1981; Manley, 1992; Davis and McPhie, 1996; Watkins et al., 2008; Gardner et al., 2012; Clay et al., 2013).

percentage of the total population (5.3%). Despite type 3 spherulites having the highest population of spherulites across samples, type 5 spherulites covered the highest area fraction (43.3%). Types 1 and 4 covered the smallest percentage area fraction (both 3.3%). These results show that types 3 and 5 dominate spherulite populations in obsidian, both in terms of number of spherulites and area (and volume) covered. Smaller spherulites (typically type 1) exhibit the shortest growth period, estimated at less than a day at high  $T_g$ /above  $T_g$  temperatures. Spherulite types 2 and 3 are considered to have started growing at high  $T_g$  temperatures. The average growth period of ~4 days is comparable to that calculated for Rocche Rosse spherulites (also 4 days) at temperatures  $\geq 800^\circ\text{C}$  by Clay et al. (2013). Type 5 (larger spherulites) have longer calculated growth periods, but processes of modification/re-crystallisation may be responsible for larger crystal sizes, independent of growth period. Type 4 spherulites are often spatially restricted, and thus growth periods were not calculated. This is further substantiated by plots of individual spherulite populations and histograms in Figure 11. Figure 11c-h show that types 3-5 are skewed towards more spherical spherulites, while types 1 and 2 (in particular, type 2) show a more even (and elongate) distribution. Type 1 (high temperatures above  $T_g$ ) spherulites show some elongation, while type 2 spherulites (high  $T_g$  temperatures) show the greatest degree of elongation. Spherulite types 3-5 show a more ideal spherical shape. These observations demonstrate some shape variation within each type, and that flow

deformation was at its peak at high  $T_g$  temperatures, evident by highly deformed type 2 spherulites.

## CONCLUSIONS

Examination of spherulites across the exceptionally-preserved obsidian lava domes and flows of Lipari and Vulcano show textural and geochemical heterogeneity, a result of different spherulite-forming processes. Such recrystallisation textures developed due to primary cooling, and continued throughout the cooling history of the lavas. Processes occur pre-, syn- and post-emplacement, across glass transition temperatures ( $T_g$ ). This results in five categorised spherulite types:

Type 1 spherulites - small, radial and slightly deformed spherulites, formed due to high degrees of undercooling at high  $T_g$  transition temperatures or above.

Type 2 spherulites - elongate spherulites with a surrounding brown rim, formed due to deformation (tend to form in shear zones) and/or enhanced undercooling.

Type 3 spherulites - large, spherical spherulites, often occurring individually in zones of low shear regions, formed by enhanced undercooling or deformation in low  $T_g$  transition or below  $T_g$ .

Type 4 spherulites - concentrated within fractures and faults, formed following solid state deformation.

Type 5 spherulites - partially- or fully-modified spherulites and lithophysae, with a non-radial interior, formed by vapour-infilling (low  $T_g$  transition or below).

Observations highlight the role of enhanced undercooling, deformation, flow-induced crystallisation, and

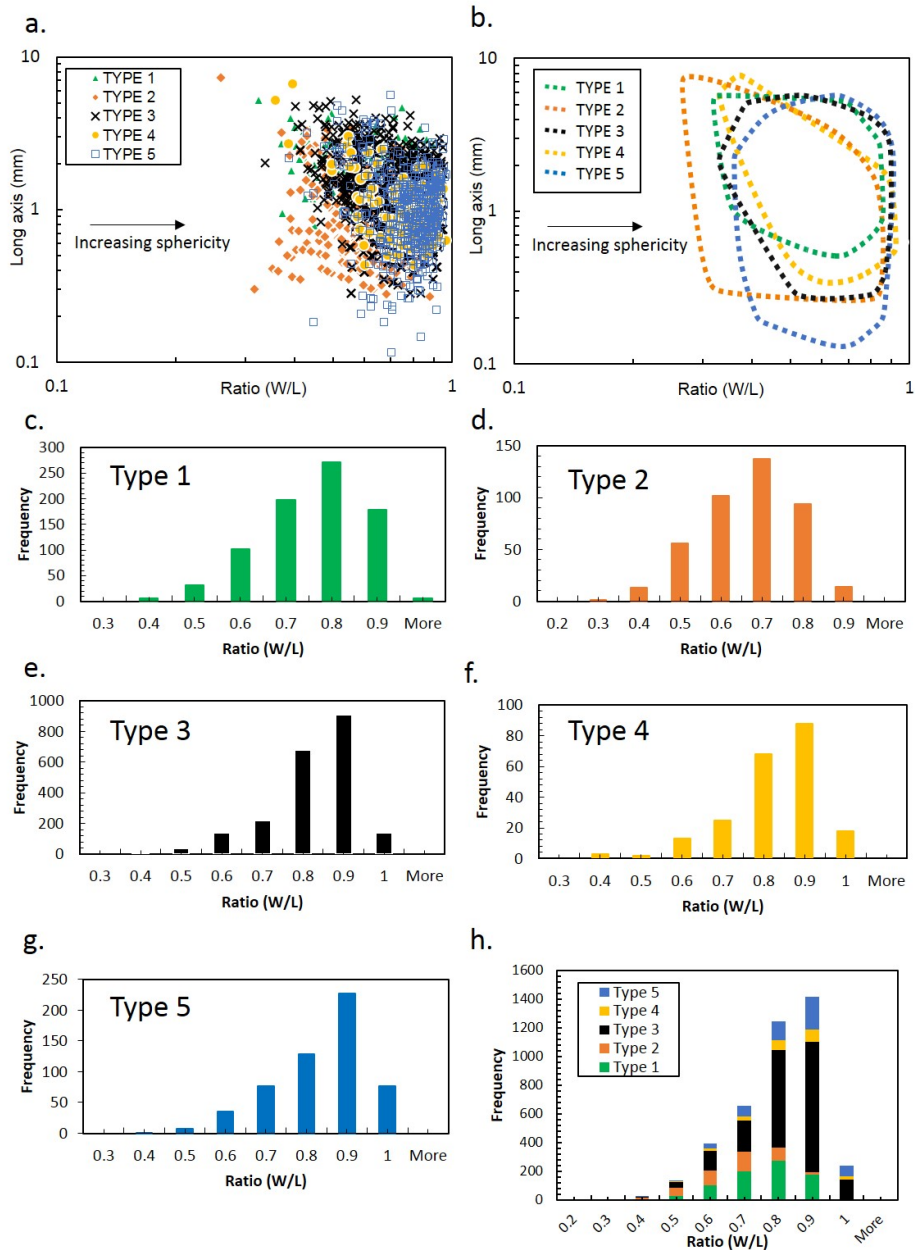


Figure 11. Individual spherulite parameters (categorised by types). (a) Plot of long axis vs. ratio of length and width (W/L) for all spherulites. (b) Representative Fields of long axis vs. W/L ratio, showing that the majority of type 2 spherulites are more elongate than other types. (c-g) Histograms for spherulite types and (h) stacked histogram of all types.

post-placement modification in the development of spherulites across  $T_g$  temperatures, and considerable spherulite heterogeneity in obsidian lavas.

#### ACKNOWLEDGEMENTS

The authors wish to gratefully acknowledge Andy Tindle (The Open University) for assistance with EMP analyses, and Richard Darton and David Evans (Keele University) for assistance with XRD and Prof Alun Vaughan and Nicola Freebody (University of Southampton) with Raman analyses. LAB is grateful to

Sophie Blanchard for support with MATLAB. The authors acknowledge support from Keele University, and grants from the Mineralogical Society (UK and Ireland) and Volcanic and Magmatic Studies Group. The authors thank Silvio Mollo and Francesca Forni for their detailed and helpful comments.

#### REFERENCES

Arrighi S., Tanguy J., Rosi M., 2006. Eruptions of the last 2200 years at Vulcano and Vulcanello (Aeolian Islands, Italy) dated by high-accuracy archaeomagnetic. *Physics of the Earth and Planetary Interiors* 159, 225-233.

- Bigazzi G. and Bonadonna F.P., 1973. Fission track dating of the obsidian of Lipari Island (Italy). *Nature* 242, 322-323.
- Binsbergen F.L., 1966. Orientation-induced Nucleation in Polymer Crystallization. *Letters to Nature* 211, 516-517.
- Breitkreuz C., 2001. Introduction to physical volcanology and volcanic textures. CVT Short course, TU Bergakademie Freiberg, Germany.
- Breitkreuz C., 2013. Spherulites and lithophysae - 200 years of investigation on high-temperature crystallization domains in silica-rich volcanic rocks. *Bulletin of Volcanology* 75, 1-16.
- Bullock L.A., 2015. Structure, emplacement and textural evolution of young obsidian lavas in the Aeolian Islands, Italy. Unpublished PhD thesis, Keele University, UK.
- Castro J.M., Beck P., Tuffen H., Nichols A.R.L., Martin M., 2008. Timescales of spherulite crystallization in obsidian inferred from water concentration profiles. *American Mineralogist* 93, 1816-1822.
- Castro J.M., Cottrell E., Tuffen H., Logan A.V., Kelley K.A., 2009. Spherulite crystallisation induces Fe-redox redistribution in silicic melt. *Chemical Geology* 268, 272-280.
- Clay P.L., O'Driscoll B., Gertisser R., Busemann H., Sherlock S.C., Kelley S.P., 2013. Textural characterization, major and volatile element quantification and Ar-Ar systematics of spherulites in the Rocche Rosse obsidian flow, Lipari, Aeolian Islands: a temperature continuum growth model. *Contributions to Mineralogy and Petrology* 165, 2, 373-395.
- Coccorullo I., Pantani R., Titomanlio G., 2008. Spherulitic nucleation and growth rates in an iPP under continuous shear flow. *Macromolecules* 41, 9214-9223.
- Crisci G.M., De Rosa R., Esperanca S., Mazzuoli R., Sonnino M., 1991. Temporal evolution of a three component volcanological system: the Island of Lipari (Aeolian Arc, Southern Italy). *Bulletin of Volcanology* 53, 207-221.
- Damby D.E., Llewellyn E.W., Horwell C.J., Williamson B.J., Najorka J., Cressey G., Carpenter M., 2014. The  $\alpha$ - $\beta$  phase transition in volcanic cristobalite. *Journal of Applied Crystallography* 47, 1205-1215.
- Davi M., De Rosa R., Barca, D., 2009. A LA-ICP-MS study of minerals in the Rocche Rosse magmatic enclaves: Evidence of a mafic input triggering the latest silicic eruption of Lipari Island (Aeolian Arc, Italy). *Journal of Volcanology and Geothermal Research* 182, 45-56.
- Davi M., De Rosa R., Holtz F., 2010. Mafic enclaves in the rhyolitic products of Lipari historical eruptions; relationships with the coeval Vulcano magmas (Aeolian Islands, Italy). *Bulletin of Volcanology* 72, 991-1008.
- Davis B., McPhie J., 1996. Spherulites, quench fractures and relict perlite in a Late Devonian rhyolite dyke, Queensland, Australia. *Journal of Volcanology and Geothermal Research* 71, 1-11.
- De Astis G., La Volpe L., Peccerillo A., Civetta L., 1997. Volcanological and petrological evolution of Vulcano island (Aeolian Arc, southern Tyrrhenian Sea). *Journal of Geophysical Research* 102, 8021-8050.
- De Astis G., Lucchi F., Dellino P., La Volpe L., Tranne C.A., Frezzotti M.L., Peccerillo A., 2013. Geology, volcanic history and petrology of Vulcano (central Aeolian archipelago). In: Lucchi F., Peccerillo A., Keller J., Tranne C.A., Rossi P.L. (eds). *The Aeolian Islands Volcanoes*. Geological Society, London, *Memoirs* 37, 281-349.
- Derakhshandeh M., Hatzikiriakos S.G., 2012. Flow-Induced Crystallization of High-Density Polyethylene: The Effects of Shear & Uniaxial Extension. *Rheologica Acta* 51, 315-327.
- Downs R.T., Palmer D.C., 1994. The pressure behavior of  $\alpha$  cristobalite. *American Mineralogist* 7, 9-14.
- Ewart A., 1971. Chemical changes accompanying spherulitic crystallization in rhyolitic lavas, central volcanic region, New Zealand. *Mineralogical Magazine* 38, 424-434.
- Forni F., Ellis B.S., Bachmann O., Lucchi F., Tranne C.A., Agostini S., Dallai L., 2015. Erupted cumulate fragments in rhyolites from Lipari (Aeolian Islands). *Contributions to Mineralogy and Petrology* 170, 49.
- Forni F., Lucchi F., Peccerillo A., Tranne C.A., Rossi P.L., Frezzotti M.L., 2013. Stratigraphy and geological evolution of the Lipari volcanic complex (central Aeolian archipelago). In: Lucchi F., Peccerillo A., Keller J., Tranne C.A., Rossi P.L. (eds). *The Aeolian Islands Volcanoes*. Geological Society, London, *Memoirs* 37, 395-469.
- Frazzetta G., La Volpe L., Sheridan M.F., 1984. Evolution of the Fossa cone, Vulcano. *Journal of Volcanology and Geothermal Research* 17, 329-360.
- Gardner J.E., Befus K.S., Watkins J., Hesse M., Miller N., 2012. Compositional gradients surrounding spherulites in obsidian and their relationship to spherulite growth and lava cooling. *Bulletin of Volcanology* 74, 8, 1865-1879.
- Gioncada A., Mazzuoli R., Bisson M., Pareschi M.T., 2003. Petrology of volcanic products younger than 42 ka on the Lipari-Vulcano complex (Aeolian Islands, Italy): An example of volcanism controlled by tectonics. *Journal of Volcanology and Geothermal Research* 122, 91-220.
- Gonnermann H.M., Manga M., 2003. Flow banding in obsidian: A record of evolving textural heterogeneity during magma deformation. *Earth and Planetary Science Letters* 236, 135-147.
- Gottsmann, J., Dingwell, D.B., 2001a. Cooling dynamics of spatter-fed phonolite obsidian flows on Tenerife, Canary Islands. *Journal of Volcanology and Geothermal Research* 105, 323-342.
- Gottsmann J., Dingwell D.B., 2001b. The cooling of frontal flow ramps: a calorimetric study on the Rocche Rosse rhyolite flow, Lipari, Aeolian Island, Italy. *Terra Nova* 13, 157-164.
- Graham R.S., Olmsted P.D., 2010. Coarse-grained simulations of flow-induced nucleation in semicrystalline polymers. *Physical Review Letters* 103, 115702.
- Higgins M.D., 2000. Measurement of Crystal size distributions. *American Mineralogist* 85, 1105-1116.
- Higgins M.D., 2002. Closure in crystal size distributions (CSD), verification of CSD calculations, and the significance of CSD fans. *American Mineralogist* 87, 171-175.
- Higgins M.D., 2006. Quantitative textural measurements in igneous and metamorphic petrology. 1<sup>st</sup> edition. Cambridge University Press.
- Hoffman J.D., Frolen L.J., Ross G.S., Lauritzen Jr J.I., 1975. On the Growth Rate of Spherulites and Axialites from the Melt in Polyethylene Fractions: Regime I and Regime II Crystallization. *Journal of Research of the National Bureau of Standards - A. Physics and Chemistry* 79A, 671-699.
- Hoffman J.D., Miller R.L., 1997. Kinetic of crystallization from the melt and chain folding in polyethylene fractions revisited: theory and experiment. *Polymer* 38, 13, 3151-3212.



- Holzhey G., 2001. Contribution to petrochemical-mineralogical characterization of alteration processes within the marginal facies of rhyolitic volcanics of Lower Permian age, Thuringian Forest, Germany. *Chemie der Erde* 61, 149-186.
- Iezzi G., Ventura G., 2005. The kinematics of lava flows inferred from structural analysis of enclaves: a review. In: Kinematics and dynamics of lava flows. Manga M., Ventura G. (eds). Geological Society of America Special Paper 396, 15-28.
- Janeschitz-Kriegl H., Ratajski E., Stadlbauer M., 2003. Flow as an effective promoter of nucleation in polymer melts: A quantitative evaluation. *Rheologica Acta* 42, 355-364.
- Keith H.D., Padden F.J., 1963. A Phenomenological Theory of Spherulitic Crystallization. *Journal of Applied Physics* 34, 2409-2421.
- Keller A., Kolnaar H.W., 1997. Flow induced orientation and structure formation. In: Meijer H.E.H. (ed). *Processing of Polymers* 18, VCH, New York, 189-268.
- Keller J., 1970. Die historischen Eruptionen von Vulcano und Lipari. *Zeitschrift der Deutschen Geologischen Gesellschaft* 121, 179-185.
- Keller J., 2002. Lipari's fiery past: dating the medieval pumice eruption of Monte Pelato. International Conference "The fire between air and water", UNESCO-Regione Siciliana, Lipari, 29 September-2 October 2002.
- Kirkpatrick R., 1975. Crystal growth from the melt: a review. *American Mineralogist* 60, 798-814.
- Kornfield J.A., Kumaraswamy G., Issaian A.M., 2002. Recent advances in understanding flow effects on polymer crystallization. *Industrial & Engineering Chemistry Research* 41, 6383-6392.
- Lauritzen Jr J.I., Hoffman J.D., 1973. Extension of theory of growth of chain-folded polymer crystals to large undercoolings. *Journal of Applied Physics* 44, 10, 4340-4352.
- Le Bas M.J., Lemaître R.W., Streckeisen A., Zanettin, B., 1986. A Chemical Classification of Volcanic-Rocks Based on the Total Alkali Silica Diagram. *Journal of Petrology* 27, 3, 745-750.
- Lofgren G.E., 1971a. Experimentally produced devitrification textures in natural rhyolite glass. *Geological Society of America Bulletin* 82, 111-124.
- Lofgren G.E., 1971b. Spherulitic textures in glassy and crystalline rocks. *Journal of Geophysical Research* 76, 23, 5635-5648.
- Lucchi F., Tranne C.A., Forni F., Rossi P.L., 2013. Geological map of the island of Lipari, scale 1:10,000 (Aeolian archipelago). In: Lucchi F., Peccerillo A., Keller J., Tranne C.A., Rossi P.L. (eds), *The Aeolian Islands Volcanoes*. Geological Society, London, Memoirs 37.
- Lucchi F., Tranne C.A., Rossi P.L., 2010. Stratigraphic approach to geological mapping of the late Quaternary volcanic island of Lipari (Aeolian Archipelago, southern Italy). *The Geological Society of America* 464, 1-33.
- Manley C.H., 1992. Extended cooling and viscous flow of large, hot rhyolite lavas: implications of numerical modeling results. *Journal of Volcanology and Geothermal Research* 53, 27-46.
- Manley C.H., Fink J.H., 1987. Internal textures of rhyolite flows as revealed by research drilling. *Geology (Boulder)* 15, 6, 549-552.
- Marsh B.D., 1988. Crystal size distributions (CSD) in rocks and the kinetics and dynamics of crystallization I: Theory. *Contributions to Mineralogy and Petrology* 99, 277-291.
- Marsh B.D., 1998. On the interpretations of Crystal Size Distributions in Magmatic Systems. *Journal of Petrology* 39, 4, 553-599.
- McArthur A.N., Cas R.A.F., Orton G.J., 1998. Distribution and significance of crystalline, perlitic and vesicular textures in the Ordovician Garth Tuff (Wales). *Bulletin of Volcanology* 60, 260-285.
- Mercalli G., Silvestri O., 1891. Le eruzioni dell'isola di Vulcano, incominciate il 3 Agosto 1888 e terminate il 22 Marzo 1890. *Relazione Scientifica. Annali dell'Ufficio Centrale di Meteorologia e Geodinamica* 10, 4, 1-213.
- Morgan D., Jerram D.A., 2006. On estimating crystal shape for crystal size distribution analysis. *Journal of Volcanology and Geothermal Research* 154, 1-2, 1-7.
- Pichler H., 1976. Carta geologica dell'Isola di Lipari (scala 1:10,000). Firenze, Litografia Artistica Cartografica.
- Piochi M., De Astis G., Petrelli M., Ventura G., Sulpizio R., Zanetti A., 2009. Constraining the recent plumbing system of Vulcano (Aeolian Arc, Italy) by textural, petrological, and fractal analysis: The 1739 A.D. Pietre Cotte lava flow. *Geochemistry, Geophysics, Geosystems*, 10, No Q01009.
- Polacci M., Papale P., 1997. The evolution of lava flows from ephemeral vents at Mount Etna: insights from vesicle distribution and morphological studies. *Journal of Volcanology and Geothermal Research* 76, 1-17.
- Richnow J., 1999. Eruptive and post-eruptive processes in rhyolite domes. Published PhD thesis, University of Canterbury, New Zealand.
- Rust A.C., Manga M., Cashman K.V., 2003. Determining flow type, shear rate and shear stress in magmas from bubble shapes and orientations. *Journal of Volcanology and Geothermal Research* 122, 111-132.
- Ryabov V.V., Grib D.E., 2005. Multiphase dykes: Signature of diverse spreading in the Northern Siberian Craton. *Russian Geology and Geophysics* 46, 5, 471-485.
- Ryan M., Sammis C., 1981. The glass transition in basalt. *Journal of Geophysical Research* 86, 9515-9535.
- Schneider C.A., Rasband W.S., Eliceiri K.W., 2012. NIH Image to ImageJ: 25 years of image analysis. *Nature Methods* 9, 671-675.
- Seaman S.J., Dyar M., Marinkovic N., 2009. The effects of heterogeneity in magma water concentration on the development of flow banding and spherulites in rhyolitic lava. *Journal of Volcanology and Geothermal Research* 183, 157-169.
- Sisson T.W., Bacon C.R., 1999. Gas-driven filter-pressing in magmas. *Geology* 27, 613-616.
- Shtukenberg A.G., Punin Y.O., Gunn E., Kahr B., 2012. Spherulites. *Chemical Reviews* 112, 1805-1838.
- Stadlbauer M., Janeschitz-Kriegl H., Eder G., Ratajski E., 2004. New extensional rheometer for creep flow at high tensile stress. Part II. Flow induced nucleation for the crystallization of iPP. *Journal of Rheology* 48, 631-639.
- Swanson S., 1977. Relation of nucleation and crystal-growth rate to the development of granitic textures. *American Mineralogist* 62, 966-978.
- Swanson S., Naney M., Westrich H., Eichelberger J., 1989. Crystallization history of Obsidian Dome, Inyo Domes, California. *Bulletin of Volcanology* 51, 161-176.

- Swainson I.P., Dove M.T., 1995. Molecular dynamics simulation of alpha- and beta-cristobalite. *Journal of Physics: Condensed Matter* 7, 1771-1788.
- Tanguy J.C., Le Goff M., Principe C., Arrighi S., Chillemi V., Paiotti A., La Delfa S., Patanè G., 2003. Archaeomagnetic dating of Mediterranean volcanics of the last 2100 years: validity and limits. *Earth and Planetary Science Letters* 211, 111-124.
- Tranne C.A., Lucchi F., Calanchi N., Lanzafame G., Rossi P.L., 2002. Geological map of the Island of Lipari. (Aeolian Islands), Scale 1:10,000. University of Bologna and INGV, LAC, Firenze.
- Tuffen H., Dingwell D.B., 2005. Fault textures in volcanic conduits: Evidence for seismic trigger mechanisms during silicic eruptions. *Bulletin of Volcanology* 67, 370-387.
- Tuffen H., Dingwell D.B., Pinkerton H., 2003. Repeated fracture and healing of silicic magma generate flow banding and earthquakes? *Geology* 31, 12, 1089-1092.
- Tuffen, H., Castro, J.M., Schipper, I., James, M.R., 2012. Observations of obsidian lava flow emplacement at Puyehue-Cordón Caulle, Chile. EGU General Assembly, Vienna, Austria, 22 April–27 April 2012, p.11451.
- Vasseur J., Wadsworth F.B., Lavallée Y., Hess K.U., Dingwell D.B., 2013. Volcanic sintering: Timescales of viscous densification and strength recovery, *Geophysical Research Letters* 40, 5658-5664.
- Ventura G., 2004. The strain path and kinematics of lava domes: an example from Lipari (Aeolian Islands, Southern Tyrrhenian Sea, Italy). *Journal of Geophysical Research* 109, B01203.
- Ventura G., 2013. Kinematics of the Aeolian volcanism (Southern Tyrrhenian Sea) from geophysical and geological data. In: Lucchi F., Peccerillo A., Keller J., Tranne C.A., Rossi P. L. (eds), *The Aeolian Islands Volcanoes*. Geological Society, London, *Memoirs* 37, 3-11.
- Voltaggio M., Branca M., Tuccimei P., Tecce F., 1995. Leaching procedure used in dating young potassic volcanic rocks by the  $^{226}\text{Ra}/^{230}\text{Th}$  method. *Earth and Planetary Science Letters* 136, 123-131.
- Watkins J., Manga M., Huber C., Martin M., 2008. Diffusion-controlled spherulite growth in obsidian inferred from  $\text{H}_2\text{O}$  concentration profiles. *Contributions to Mineralogy and Petrology* 157, 2, 163-172.
- Westrich H., Stockman H., Eichelberger J., 1988. Degassing of rhyolitic magma during ascent and emplacement. *Journal of Geophysical Research* 93, 6503-6511.
- Wright A.F., Leadbetter A.J., 1975. The structures of the  $\beta$ -cristobalite phases  $\text{SiO}_2$  and  $\text{AlPO}_4$ . *Philosophical Magazine* 31, 1391-1401.